Two-Layer-Based Multiarms Bilateral Teleoperation Architecture

Marco Minelli, *Member, IEEE*, Nicola Piccinelli, Fabio Falezza, Federica Ferraguti, Riccardo Muradore, *Member, IEEE*, and Cristian Secchi, *Senior Member, IEEE*

***Abstract*— In this article, we propose a novel bilateral teleoperation architecture for a multiarms system based on the two-layer approach. Exploiting the concept of shared energy tank, a passivity layer guarantees the passivity of the overall architecture with respect to destabilizing factors such as time delays in the communication channel. The desired behavior can then be freely designed in the transparency layer. The formulation of the energy tank is first revised, allowing a more efficient use of energy, and then extended, allowing explicitly the use of both admittance and impedance causality robots. A novel framework capable of combining the use of teleoperated and autonomous robots is proposed. The architecture has been tested and validated on a multiarms system in a realistic surgical scenario with the da Vinci research kit (dVRK) and an autonomous arm holding the endoscope.**

***Index Terms*— Control architectures and programming, medical robots and systems, surgical robotics: laparoscopy, telerobotics and teleoperation.**

I. Introduction

TELEOPERATION systems allow the user to interact with a remote environment performing a task while increasing safety and accuracy. An example of this kind of task is the manipulation of dangerous material, such as chemical substances. The standard architecture of a teleoperation system includes a local device and a remote device. The local device is located at the operator side and is used to measure and send the operator movements to the remote device, in the form of pose information. The remote device is located in the remote environment and replicates the motion of the local device, performing the task. In a bilateral teleoperation architecture, the interaction wrench between the remote device and the environment is measured or estimated and sent back to the local device, in the form of force feedback. The local device is then able to replicate the interaction with the environment, providing the user with the feeling of directly interacting with the remote environment. Bilateral teleoperation has been exploited for many applications like bomb disposal [1] and surgical procedures [2].

A teleoperation architecture composed of a single local device and a single remote device (SLSR) may not provide the necessary dexterity and flexibility for accomplishing a task in a remote environment. In these cases, a teleoperation architecture composed of multiple local devices and multiple remote devices (MLMR) can provide the desired level of remote mobility and interaction capabilities. A well-known example of the application of an MLMR teleoperation architecture is the da Vinci Surgical System (Intuitive Surgical, Inc., Sunnyvale, CA, USA).[1] The surgeon uses two hand-held haptic interfaces to teleoperate three or four arms of the surgical robot for performing complex tasks.

Stability and transparency are the main issues when designing a bilateral teleoperation system. Due to the distance between the devices, the exchange of information between the local and the remote sides typically happens over a delayed communication channel. Communication delays and interaction with a poorly known environment are the main sources of instability in any teleoperation architecture. As it will be shown in Section II, several control algorithms have been proposed in the literature to solve the stability problem. However, these algorithms typically decrease the transparency of the system, i.e., the measure of how well the desired motion and force feedback are implemented at the remote and local sides, respectively [3].

In this article, we aim at developing an MLMR bilateral teleoperation architecture which guarantees a stable interaction with a poorly known environment (e.g., the human body) while allowing the user to change the kind of feedback. Our methodology is built on top of the shared energy tank for MLMR bilateral teleoperation architecture proposed in [4]. In fact, as in [4], we augment each side of the teleoperation system with a shared energy tank, and we interconnect each robot on the same side to the same tank. The tank communicates with the other side using the communication channel also used for signals and commands. To overcome the limitations in [4] (see Section II for more details), we first develop a novel energy transfer protocol that minimizes the waste of energy, and then, we formulate a novel tank dynamics to

Manuscript received 7 June 2022; revised 22 October 2022; accepted 28 October 2022. Date of publication 15 December 2022; date of current version 25 April 2023. This work was supported by the European Union's Horizon 2020 Research and Innovation Program (SARAS) under Agreement 779813. Recommended by Associate Editor S. Pirozzi. *(Corresponding author: Marco Minelli.)*

Marco Minelli, Federica Ferraguti, and Cristian Secchi are with the Department of Sciences and Methods of Engineering, University of Modena and Reggio Emilia, 41121 Modena, Italy (e-mail: marco.minelli@unimore.it; federica.ferraguti@unimore.it; cristian.secchi@unimore.it).

Nicola Piccinelli, Fabio Falezza, and Riccardo Muradore are with the Altair Laboratory, Department of Computer Science, University of Verona, 37129 Verona, Italy (e-mail: nicola.piccinelli@univr.it; fabio.falezza@univr.it; riccardo.muradore@univr.it).

Color versions of one or more figures in this article are available at https://doi.org/10.1109/TCST.2022.3225732.

Digital Object Identifier 10.1109/TCST.2022.3225732

[1] https://www.intuitive.com/

implement it. Moreover, we extend the formulation of the overall teleoperation architecture considering a generic number of both admittance and impedance causality manipulators on each side. Finally, we experimentally validate the proposed architecture on surgical training tasks. The main contributions of this article are as follows.

1) A novel theoretical formulation of the shared energy tank to improve energy consumption and allow a consistent flow of energy among all the actors of the teleoperation architecture exploiting the energy-transfer protocol.
2) A revised methodology to let the teleoperation architecture work with a generic number of both admittance and impedance causality manipulators, and allow the collaboration between teleoperated and autonomous arms.
3) An experimental validation of the proposed architecture on surgical training tasks.

This article is organized as follows. Section II reports different approaches addressing the stability/transparency problem in SLSR bilateral teleoperation architecture and how these approaches have been extended to MLMR bilateral teleoperation architectures. Section III presents the modeling of the devices involved in the system and how they are augmented with the proposed shared energy tank. The overall bilateral control architecture is described in Section IV while Section V reports simulations showing the advantages of the novel formulation on the energy dynamics. Section VI shows the experimental setup and the results of the validation of the proposed teleoperation architecture. Finally, conclusion are reported in Section VII.

II. Related Works

Several control architectures have been proposed for implementing a bilateral teleoperation system [5]. In this section, we will focus on the works that specifically address the design of a stable and transparent MLMR teleoperation architecture with respect to time delays and interaction with poorly known environments.

Passivity-based control strategies have been proven to be very successful since they allow to robustly handle the interaction with unstructured environments and to compensate for the destabilizing effects of the communication delay. For example, the wave variables developed by Niemeyer and Slotine [6] are one of the main tools used to achieve a stable teleoperation system and have been exploited for decades. Based on a given scheme, the wave variables encrypt the power variables (velocities and forces) exchanged between the local and the remote sides to turn the communication channel into a passive element, regardless of the time delays. Furthermore, if both the local and remote sides are passive, the overall teleoperation architecture is passive too and thus stable. An example of MLMR application of this concept has been developed by Huang et al. [7]. Based on the forward wave compensation method [8], a backward wave compensation method and an energy regulator [9], they developed a DLDR teleoperation system. An asymmetric compensation method enhances the velocity and force tracking performance while ensuring the passivity of the system. The main drawback of wave variables is that the inherent dynamics of wave-based communication channels is often deleterious for the transparency of the teleoperation system.

Starting from the time domain passivity control (TDPC) algorithm developed by Hannaford and Ryu [10], Ryu et al. [11] proposed an application to bilateral telemanipulation. In their approach, two elements are introduced: 1) the passivity observer (PO) and 2) the passivity controller (PC). The PO monitors the energy flow into the system and a time-varying damping element, the PC, is activated to dissipate the excessive energy when necessary. An improved version of this kind of architecture, the power-based TDPC (PTDPC), has been proposed by Ye et al. [12], where the power flow, rather than the energy flow, is monitored to achieve a smoother activation of the PC. An example of MLMR implementation of the PTDPC has been developed by Chen et al. [13]. In particular, the SLSR PTDPC architecture is extended to solve the passivity problem in an MLMR scenario and a novel communication structure allows the system to deal with the complexity of the communication channel when multiple local and remote devices are interconnected. The main drawback of these kinds of approaches is related to the conservativeness of the resulting system, often too high and deleterious for transparency.

Alternative approaches are based on the idea of predicting the nondelayed output of the plant by exploiting a model of the system, and so compensating for the problem introduced by the delays. Smith [14] first proposed a linear predictive controller known as *Smith predictor*. In a teleoperation system, the local and the remote devices are haptic interfaces or robotic manipulators, which model is typically nonlinear and may also vary with time (e.g., in the case of user interaction or object picking). Huang and Lewis [15] introduced a recurrent neural network to capture the remote robot nonlinearity and integrated it with a linear Smith predictor to improve the performance of the system. With the use of a Slotine-Li adaptive control algorithm [16], Fite et al. [17] developed an architecture which can also deal with time-varying environment dynamics. Smith and Van Hashtrudi-Zaad [18] introduced the online training of the network, allowing the system to estimate and map the remote device and environment dynamics at the local side. This increases the usability of the system, especially in the presence of substantial delays in the communication channel. The online knowledge of the remote and environment dynamics allows the system to work also if the environment dynamics is nonlinear and time-varying. These techniques are very promising but, unfortunately, examples of application can be found only for trilateral scenarios, as in [19] and [20], with a particular focus on the dual-local single-remote teleoperation architecture.

A different approach consists of replacing the force rendered to the user with a different type of feedback, such as audio, visual, or cutaneous. This technique, called sensory substitution [21], allows to make the system intrinsically stable since the local devices are used as kinematic systems to produce only the control signals for the remote devices (i.e., unilateral

teleoperation). However, it is well known that this technique reports worse performance in terms of transparency. Similarly, Prattichizzo et al. [22] proposed to substitute haptic force feedback with cutaneous feedback only. This technique, called sensory subtraction, reports higher transparency levels since the force generated is perceived as a subtraction between the complete haptic interaction and the kinesthetic part of it.

Although it has been shown that these techniques can produce effective feedback to the user, the goal of this article is to propose an architecture that solves the stability problem in systems capable of reproducing force feedback.

Franken et al. [23] developed a teleoperation control architecture based on a two-layer framework. By exploiting the concept of energy tank, this kind of approach splits the control architecture into two hierarchical layers. The higher layer is used to implement a strategy that addresses the desired transparency while the lower layer ensures that passivity is not violated. An example of the application of this kind of technique for an SLSR teleoperation architecture has been developed by Ferraguti et al. [24], where the two-layer framework has been exploited to passively implement the SLSR bilateral teleoperation architecture and to compensate the position mismatch between the local and the remote device. Extensions to single-local multiremote teleoperation systems were also proposed, for example, by Secchi et al. [25].

The two-layer architecture has been extended also to MLMR systems by Minelli et al. [4] by introducing the concept of a shared energy tank. In this approach, a single tank is placed at each side of the teleoperation architecture and all devices belonging to the same side share the energy inside the same tank. This allows the system to decrease the conservativeness introduced by passivity preservation and to increase transparency. Even though this architecture guarantees the stability of the system while allowing a high level of flexibility and transparency, there are some lacks from the energy management point of view: energy is often wasted when the energy tank needs to be bounded. Moreover, the formulation of the shared energy tank considers each side of the teleoperation system made up of only admittance causality robots, restricting its field of use to torque/force-controlled robots. The experimental validation was done in laboratory scenarios with industrial robots.

III. Local and Remote Side

We consider a teleoperation system composed of N_l local robots and N_r remote robots, fully actuated and locally gravity compensated. Each side is composed of a generic number of admittance causality robots (N_l^f for the local side and N_r^f for the remote side) and a generic number of impedance causality robots (N_l^v for the local side and N_r^v for the remote side). We consider $N_l \leq N_r$, where each arm at the local side controls just one arm at the remote side and the remaining $N_r - N_l$ arms are autonomous. Each robot is modeled as an n-DOFs Euler-Lagrange system,[2] where the control input depends on the causality of the robot.

[2]For ease of notation, we consider that all the robots have the same number of DOFs. All the results can be easily generalized to the case where the robots have a different number of DOFs.

With a slight abuse of notation and for clarity of presentation, we will omit the dependencies of the variables when the context is clear.

Admittance causality robots can be controlled by directly providing the control force and can be modeled as

$$\Lambda_{s_i}^f \ddot{x}_{s_i}^f + \mu_{s_i}^f \dot{x}_{s_i}^f = F_{s_i}^f + E_{s_i}^f \tag{1}$$

where $x_{s_i}^f \in \mathbb{R}^n$ are the coordinates of the configuration of the end-effector in the task space with $i = 1, \ldots, N_s^f$ and $s \in \{l, r\}$. The subscripts l and r are used to indicate the local and the remote side, respectively. The term $\Lambda_{s_i}^f \in \mathbb{R}^{n\times n}$ is the symmetric and positive-definite inertia matrix, $\mu_{w_i}^f \in \mathbb{R}^{n\times n}$ is the Coriolis/centrifugal matrix. The term $F_{s_i}^f \in \mathbb{R}^n$ represents the control inputs vector while $E_{s_i}^f \in \mathbb{R}^n$ is the vector of generalized external forces (i.e., the force applied by the user or the force applied by the environment).

Impedance causality robots can be controlled by providing the control velocity and can be modeled as

$$\Lambda_{s_j}^v \ddot{x}_{s_j}^v + \mu_{s_j}^v \dot{x}_{s_j}^v = F_{s_j}^v\left({}^\tau\dot{x}_{s_j}^v\right) + E_{s_j}^v \tag{2}$$

where $x_{s_j}^v \in \mathbb{R}^n$ are the coordinates of the configuration of the end-effector in the task space with $j = 1, \ldots, N_s^v$. The term $\Lambda_{s_j}^v \in \mathbb{R}^{n\times n}$ is the symmetric and positive-definite inertia matrix, $\mu_{s_j}^v \in \mathbb{R}^{n\times n}$ is the Coriolis/centrifugal matrix. The term $F_{w_j}^v \in \mathbb{R}^n$ represents the control force due to the control input velocity vector ${}^\tau\dot{x}_{s_j}^v \in \mathbb{R}^n$, and $E_{s_j}^v \in \mathbb{R}^n$ is the vector of generalized external forces.

It is worth noting that impedance causality robots do not allow the user to directly command the control force $F_{s_j}^v$ but only the control velocity ${}^\tau\dot{x}_{s_j}^v$. The term $F_{s_j}^v({}^\tau\dot{x}_{s_j}^v)$ is computed by an inner controller which takes care of tracking the desired velocity ${}^\tau\dot{x}_{s_j}^v$. However, the term $F_{s_j}^v({}^\tau\dot{x}_{s_j}^v)$ is typically measurable, allowing the control of power flowing from the controller to the robot.

The modeling of each side of the teleoperation system is a generic composition of multiple devices with different causality. The proposed methodology can be used to control a generic robotic system made up of teleoperated and autonomous arms, improving the flexibility of the proposed architecture.

To passively implement the bilateral teleoperation architecture, shared energy tanks are introduced in the system at the local and remote sides. Based on the original idea of the energy tank [26], all the robots on the same side are connected to a shared energy tank such that they can fill or extract energy from the tank to implement the desired behavior.

To be able to fill the tank when necessary, a controlled dissipation is implemented on each admittance-controlled robot, and the corresponding dissipated energy flows into the tank. This can be done by splitting the control input of each admittance-controlled robot into the sum of two terms

$$F_{s_i}^f = {}^dF_{s_i}^f + {}^\tau F_{s_i}^f \tag{3}$$

where the first term implements a variable local damping by setting

$${}^dF_{s_i}^f = -D_{s_i}^f \dot{x}_{s_i}^f \tag{4}$$

with $D_{s_i}^f \in \mathbb{R}^{n\times n}$ a time-varying positive semidefinite matrix. The second term is the effective control input.

By embedding the damping injection (4) into (1) we get the following damped Euler–Lagrange model for each admittance causality robot:

$$\Lambda_{s_i}^f \ddot{x}_{s_i}^f + \mu_{s_i}^f \dot{x}_{s_i}^f + D_{s_i}^f \dot{x}_{s_i}^f = {}^\tau F_{s_i}^f + E_{s_i}^f. \tag{5}$$

The damping injection mechanism is implemented only on the admittance causality robots since they allow the implementation of an external force, which cannot be done on impedance causality robots.

A shared energy tank is then introduced. As described in [27], it is necessary not to store excessive energy in the tank to avoid the implementation of practically unstable behaviors.

With respect to the formulation of the shared energy tank in [4], we propose the following formulation:

$$\begin{cases} \dot{x}_{t_s} = \sigma_s \left(\displaystyle\sum_{i=1}^{N_s^f} \frac{(\dot{x}_{s_i}^f)^T \, D_{s_i}^f \, \dot{x}_{s_i}^f}{x_{t_s}} + u_{t_s} \right) & \text{(6a)} \\ y_{t_s} = \dfrac{\partial T_s}{\partial x_{t_s}} & \text{(6b)} \end{cases}$$

where $x_{t_s} \in \mathbb{R}$ is the state of the tank, $\sigma_s \in \{0, 1\}$ is a flag used to limit the energy stored in the tank, $(u_{t_s}, y_{t_s}) \in \mathbb{R} \times \mathbb{R}$ is the power port through which the tank can exchange energy with the rest of the world, and

$$T_s\left(x_{t_s}\right) = \frac{1}{2} x_{t_s}^2 \tag{7}$$

is the energy stored in the tank.

Each robot is interconnected to the energy tank to use the energy stored to execute the desired action. This can be done by implementing the following power-preserving interconnection between all the robots and the shared energy tank

$$\begin{cases} {}^\tau F_{s_i}^f = \omega_{s_i}^f \, y_{t_s} & \text{(8a)} \\ {}^\tau \dot{x}_{s_j}^v = \omega_{s_j}^v \, y_{t_s} & \text{(8b)} \\ u_{t_s} = -\displaystyle\sum_{i=1}^{N_s^f} \left(\omega_{s_i}^f\right)^T \dot{x}_{s_i}^f - \sum_{j=1}^{N_s^v} \left(\omega_{w_s}^v\right)^T F_{s_j}^v & \text{(8c)} \end{cases}$$

for $i = 1, \ldots, N_s^f$ and $j = 1, \ldots, N_s^v$. Substituting (8a) and (8b) in (8c), the following equation holds:

$$\sum_{i=1}^{N_s^f} \left(\dot{x}_{s_i}^f\right)^T \, {}^\tau F_{s_i}^f + \sum_{j=1}^{N_s^v} \left(F_{s_j}^v\right)^T \, {}^\tau \dot{x}_{s_j}^v = -u_{t_s} y_{t_s} \tag{9}$$

which means that each robot can extract/inject energy from/into the tank to implement the desired input by properly choosing the modulation factors $\omega_{s_i}^f, \omega_{s_j}^v \in \mathbb{R}^n$. Let now set

$$\Lambda_s^f = \operatorname{diag}\left(\Lambda_{s_1}^f \; \ldots \; \Lambda_{s_{N_s^f}}^f\right) \tag{10}$$

$$\mu_s^f = \operatorname{diag}\left(\mu_{s_1}^f \; \ldots \; \mu_{s_{N_s^f}}^f\right) \tag{11}$$

$$D_s^f = \operatorname{diag}\left(D_{s_1}^f \; \ldots \; D_{s_{N_s^f}}^f\right) \tag{12}$$

$$x_s^f = \left[x_{s_1}^f \; x_{s_2}^f \; \ldots \; x_{s_{N_s^f}}^f\right] \tag{13}$$

$$\omega_s^f = \left[\omega_{s_1}^f \; \omega_{s_2}^f \; \ldots \; \omega_{s_{N_s^f}}^f\right] \tag{14}$$

$$E_s^f = \left[E_{s_1}^f \; E_{s_2}^f \; \ldots \; E_{s_{N_s^f}}^f\right] \tag{15}$$

and

$$\Lambda_s^v = \operatorname{diag}\left(\Lambda_{s_1}^v \; \ldots \; \Lambda_{s_{N_s^v}}^v\right) \tag{16}$$

$$\mu_s^v = \operatorname{diag}\left(\mu_{s_1}^v \; \ldots \; \mu_{s_{N_s^v}}^v\right) \tag{17}$$

$$D_s^v = \operatorname{diag}\left(D_{s_1}^v \; \ldots \; D_{s_{N_s^v}}^v\right) \tag{18}$$

$$x_s^v = \left[x_{s_1}^v \; x_{s_2}^v \; \ldots \; x_{s_{N_s^v}}^v\right] \tag{19}$$

$$\omega_s^v = \left[\omega_{s_1}^v \; \omega_{s_2}^v \; \ldots \; \omega_{s_{N_s^v}}^v\right] \tag{20}$$

$$F_s^v\left(\dot{x}_s^v\right) = \left[F_{s_1}^v\left(\dot{x}_{s_1}^v\right) \; \ldots \; F_{s_{N_s^v}}^v\left(\dot{x}_{s_{N_s^v}}^v\right)\right] \tag{21}$$

$$E_s^v = \left[E_{s_1}^v \; E_{s_2}^v \; \ldots \; E_{s_{N_s^v}}^v\right]. \tag{22}$$

By grouping (5) and by considering (6) and (8), it is possible to model each side of the MLMR teleoperation system as

$$\begin{cases} \Lambda_s^f \ddot{x}_s^f + \mu_s^f \dot{x}_s^f + D_s^f \dot{x}_s^f = \omega_s^f \, x_{t_s} + E_s^f & \text{(23a)} \\ \Lambda_s^v \ddot{x}_s^v + \mu_s^v \dot{x}_s^v = F_s^v(\omega_s^v \, x_{t_s}) + E_s^v & \text{(23b)} \\ \dot{x}_{t_s} = \sigma_s \left(\dfrac{(\dot{x}_s^f)^T \, D_s^f \, \dot{x}_s^f}{x_{t_s}} - (\omega_s^f)^T \, \dot{x}_s^f - (\omega_s^v)^T \, F_s^v \right). & \text{(23c)} \end{cases}$$

With respect to [4], we redefine the terms σ_s in (23) as

$$\sigma_s = \begin{cases} 0, & \text{if } T_s\left(x_{t_s}\right) = T_s^{\max} \wedge \Delta T_s > 0 \\ 1, & \text{otherwise} \end{cases} \tag{24}$$

where

$$\Delta T_s = \frac{\left(\dot{x}_s^f\right)^T \, D_s^f \, \dot{x}_s^f}{x_{t_s}} - \left(\omega_s^f\right)^T \, \dot{x}_s^f - \left(\omega_s^v\right)^T \, F_s^v \tag{25}$$

and $T_s^{\max}$ represents the energy upper bound. The shared energy tank proposed here allows to bound the maximum level of energy stored in the tank by energetically disconnecting the tank from the robots. It is worth noting that such disconnection occurs only when $\sigma_s = 0$, that is when

$$T_s\left(x_{t_s}\right) = T_s^{\max} \tag{26}$$

and

$$\frac{\left(\dot{x}_s^f\right)^T \, D_s^f \, \dot{x}_s^f}{x_{t_s}} - \left(\omega_s^f\right)^T \, \dot{x}_s^f - \left(\omega_s^v\right)^T \, F_s^v > 0. \tag{27}$$

This means that the energy tank is full and the overall control action is dissipative (i.e., injecting energy into the tank), and so

it is safe to decouple the tank and the robots. In this situation, the energetic disconnection between the tank and the robots allows keeping the energy stored in the tank constant to the maximum value $T_s^{\max}$, since no more energy can flow in the tank.

When $\sigma_s = 0$, the extra energy would produce an evolution of $\dot{x}_{t_s}$ represented by the term

$$\frac{\left(\dot{x}_s^f\right)^T \; D_s^f \; \dot{x}_s^f}{x_{t_s}} - \left(\omega_s^f\right)^T \; \dot{x}_s^f - \left(\omega_s^v\right)^T \; F_s^v. \tag{28}$$

Since $\sigma_s = 0$, this extra energy does not produce any effects on the tank level. We design a local damping for each robot as

$$D_s^f = \begin{cases} {}^{\min}D_s^f, & \text{if} \quad T_s\left(x_{t_s}\right) > T_s^{b_{\max}} \\ \xi\left(T_s\left(x_{t_s}\right)\right), & \text{if} \quad T_s^{b_{\min}} \leq T_s\left(x_{t_s}\right) \leq T_s^{b_{\max}} \\ {}^{\max}D_s^f, & \text{if} \quad T_s\left(x_{t_s}\right) < T_s^{b_{\min}}. \end{cases} \tag{29}$$

If the energy in the tank exceeds the energy upper threshold $T_s^{b_{\max}}$, the local damping injection of the robot is set to a minimum level ${}^{\min}D_s^f$ since harvesting energy is not needed. If the energy in the tank is going below the energy lower threshold $T_s^{b_{\min}}$, the local damping injection of the robot is set to a maximum level ${}^{\max}D_s^f$, to fill energy into the tank as quickly as possible. Otherwise $D_s^f = \xi(T_s(x_{t_s}))$, where $\xi(T) : \mathbb{R} \to \mathbb{R}^{(N_s^f n)\times(N_s^f n)}$ is any smooth non-increasing function such that $D_s^f = {}^{\min}D_s^f$ if $T_s(x_{t_s}) = T_s^{b_{\max}}$ and $D_s^f = {}^{\max}D_s^f$ if $T_s(x_{t_s}) = T_s^{b_{\min}}$.

The choice of $\xi(T_s(x_{t_s}))$ guarantees a smooth transition between ${}^{\min}D_s^f$ and ${}^{\max}D_s^f$, without discontinuities in the forces applied to the devices. As defined in (29) all the robots contribute in the same way to energy harvesting. Nevertheless, robot-specific damping strategies may be designed.

Finally, the desired input for the robots can be achieved by setting the modulating terms in (8a) and (8b) as

$$\omega_{s_i}^f = K_s\left(T_s\left(x_{t_s}\right)\right)\frac{{}^{\text{des}}F_{s_i}^f}{x_{t_s}} \tag{30}$$

and

$$\omega_{s_j}^v = K_s\left(T_s\left(x_{t_s}\right)\right)\frac{{}^{\text{des}}\dot{x}_{s_i}^v}{x_{t_s}} \tag{31}$$

where

$$K_s\left(T_s\left(x_{t_s}\right)\right) = \min\left(1, \frac{T_s\left(x_{t_s}\right) - T_s^{\min}}{T_s^R - T_s^{\min}}\right). \tag{32}$$

If the energy stored in the tank is less than the user-defined threshold $T_s^R \in \mathbb{R}$, a scaled version of the desired input is implemented. In the worst case, it results that $K_s(T(x_s)) = 0$, which implies that no commands will be implemented to preserve passivity. Nevertheless, since the local damping is set to its maximum value when $T(x_{t_s}) < T_s^{b_{\min}}$, in practice it is very unlikely that $K_s(T(x_{t_s}) = 0$ if T_s^R is set greater or equal to $T_s^{b_{\min}}$.

To ensure that the modulation introduced by the function $K_s(T(x_s)) : \mathbb{R} \to \mathbb{R}$ can only reduce the desired command, $K_s(T(x_s))$ has to be chosen such that the interval $[T_s^{\min}, T_s^{\max}]$ is mapped into the interval $[0, 1]$ and $K_s(T_s^{\min}) = 0$. These conditions prevent any energy extraction under the threshold $T_s^{\min}$, preserving passivity and avoiding (23c) to become singular.

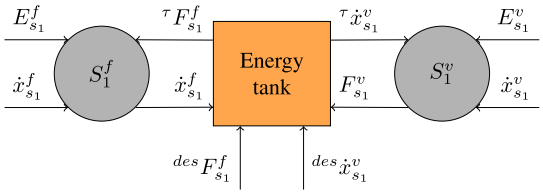

Fig. 1. Coupling of two generic local or remote devices. Device s_1^f with admittance causality, device s_1^v with impedance causality, and the energy tank. The tank is used to store the dissipated energy and/or to extract the needed energy.

It is worth noting that if impedance causality robots are used, the modulation factor (31) may cause a drift in the position tracking since the velocity is reduced. This does not hold for the admittance causality robots, since the modulation acts directly on the force.

The constants $T_s^{\min}, T_s^{\max}, T_s^{b_{\max}}, T_s^{b_{\min}}, {}^{\min}D_s^f, {}^{\max}D_s^f$ are application and robot-dependent design parameters. Fig. 1 shows the coupling of two generic local or remote devices with the energy tank.

A. Passivity of the Local and Remote Sides

The kinetic energy $V_s^f(t)$ of the system described in (23a) is given by the sum of the kinetic energies of all the admittance causality robots at the s side and can be defined as

$$V_s^f(t) = \frac{1}{2}\left(\dot{x}_s^f(t)\right)^T \; \Lambda_s^f(t) \; \dot{x}_s^f(t) \tag{33}$$

while $\dot{V}_s^f(t)$ is given by

$$\dot{V}_s^f(t) = \dot{x}_s^f(t)^T \; \Lambda_s^f(t) \; \ddot{x}_s^f(t) + \frac{1}{2} \; \dot{x}_s^f(t)^T \; \dot{\Lambda}_s^f(t) \; \dot{x}_s^f(t). \tag{34}$$

Since $\dot{\Lambda}_s^f(t) - 2\mu_s^f(t)$ is skew symmetric and using (23a) we can rewrite (34) as

$$\dot{V}_s^f(t) = x_{t_s}\left(\omega_s^f\right)^T \dot{x}_s^f + \left(\dot{x}_s^f\right)^T \; E_s^f - \left(\dot{x}_s^f\right)^T \; D_s^f \; \dot{x}_s^f. \tag{35}$$

Following the same passages, the kinetic energy $V_s^v(t)$ of the system described in (23b) is given by the sum of the kinetic energies of all the impedance causality robots at the s side and can be defined as

$$V_s^v(t) = \frac{1}{2}\left(\dot{x}_s^v(t)\right)^T \; \Lambda_s^v(t) \; \dot{x}_s^v(t) \tag{36}$$

and its time derivative can be computed as

$$\dot{V}_s^v(t) = \left(\dot{x}_s^v\right)^T \; F_s^v + \left(\dot{x}_s^v\right)^T \; E_s^v. \tag{37}$$

It is common practice, when using impedance causality robots, assuming perfect velocity tracking. This means that

$$\dot{x}_{s_j}^v = {}^{\tau}\dot{x}_{s_j}^v \tag{38}$$

which, using (8), (20), and (19) becomes

$$\dot{x}_s^v = \omega_s^v x_{t_s}. \tag{39}$$

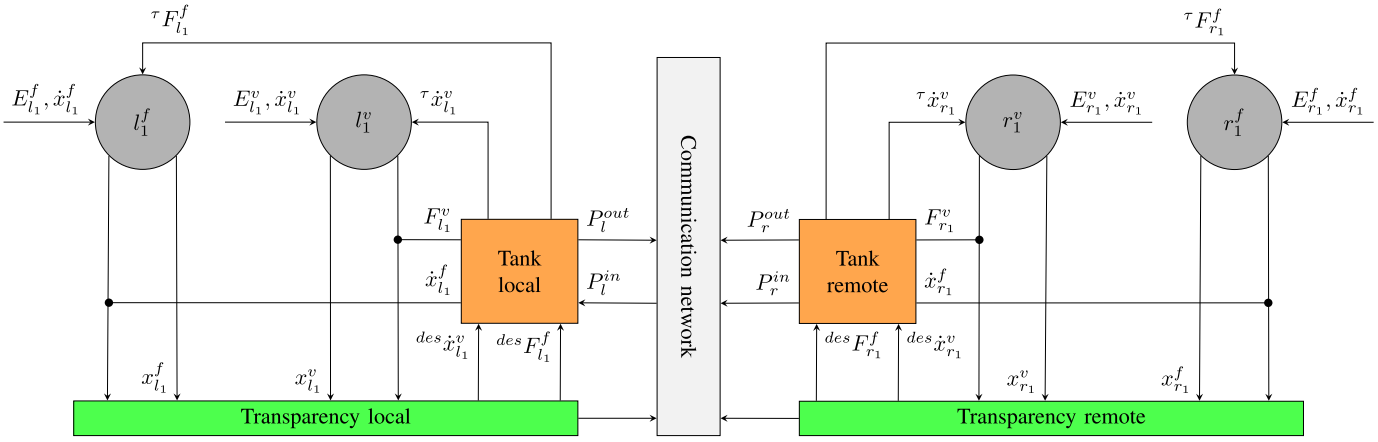

Fig. 2. Coupling of two generic local devices l_1^f and l_1^v with two remote devices r_1^f and r_1^v and one shared energy tank per side by means of the communication channel.

Equation (37) can be then rewritten as

$$\dot{V}_s^v(t) = x_{t_s} \left(\omega_s^v\right)^T F_s^v + \left(\dot{x}_s^v\right)^T E_s^v. \tag{40}$$

Finally, by substituting (23c) in (7), we can define $\dot{T}_s(t)$ as

$$\dot{T}_s(t) = \sigma_s \Big(\left(\dot{x}_s^f\right)^T D_s^f \dot{x}_s^f - x_{t_s} \left(\omega_s^f\right)^T \dot{x}_s^f - x_{t_s} \left(\omega_s^v\right)^T F_s^v \Big). \tag{41}$$

Proposition 1: The system in (23) is passive with respect to the pair $((E_{s_1}^f, \ldots, E_{s_{N_s^f}}^f, E_{s_1}^v, \ldots, E_{s_{N_s^v}}^v), (\dot{x}_{s_1}^f, \ldots, \dot{x}_{s_{N_s^f}}^f, \dot{x}_{s_1}^v, \ldots, \dot{x}_{s_{N_s^v}}^v))$.

Proof: Consider as a storage function the total energy of the teleoperation system (23)

$$\mathcal{V}(t) = V_s^f(t) + V_s^v(t) + T_s(t) \tag{42}$$

where $V_s^f(t) + V_s^v(t)$ represents the energy associated with the local or remote side and T_s the energy stored in the corresponding tank. From (42), it follows that:

$$\dot{\mathcal{V}}(t) = \dot{V}_s^f(t) + \dot{V}_s^v(t) + \dot{T}_s(t). \tag{43}$$

Substituting (35), (40), and (41) in (43), we obtain

$$\dot{\mathcal{V}}(t) = \left(\dot{x}_s^f\right)^T E_s^f + \left(\dot{x}_s^v\right)^T E_s^v - (1 - \sigma_s) \times \Big(\left(\dot{x}_s^f\right)^T D_s^f \dot{x}_s^f + -x_{t_s} \left(\omega_s^f\right)^T \dot{x}_s^f - x_{t_s} \left(\omega_s^v\right)^T F_s^v \Big). \tag{44}$$

From (24), $\sigma_s \in \{0, 1\}$, and from (25) $\sigma_s = 0$ if and only if

$$\left(\dot{x}_s^f\right)^T D_s^f \dot{x}_s^f - x_{t_s} \left(\omega_s^f\right)^T \dot{x}_s^f - x_{t_s} \left(\omega_s^v\right)^T F_s^v \geq 0.$$

Thus, it follows that:

$$\dot{\mathcal{V}}(t) \leq \sum_{i=1}^{N_s^f} \left(\dot{x}_{s_i}^f\right)^T E_{s_i}^f + \sum_{j=1}^{N_s^v} \left(\dot{x}_{s_j}^v\right)^T E_{s_j}^v \tag{45}$$

which implies the passivity condition

$$\mathcal{V}(t) - \mathcal{V}(0) \leq \int_0^t \sum_{i=1}^{N_s^f} \left(\dot{x}_{s_i}^f(\tau)\right)^T E_{s_i}^f(\tau) + \sum_{j=1}^{N_s^v} \left(\dot{x}_{s_j}^v(\tau)\right)^T E_{s_j}^v(\tau) d\tau. \tag{46}$$

□

IV. Bilateral Control Architecture

In this section, we describe the control architecture for the bilateral teleoperation of a generic MLMR system.

Following the approach proposed in [24], we endow each shared energy tank with two ports, P_s^{out} and P_s^{in}, through which the tank can send/receive extra power to/from the rest of the world. These ports allow the interconnection of the local and the remote sides using a delayed communication channel, achieving the teleoperation architecture.

Fig. 2 shows the overall architecture in the case of two local devices ($N_l = 2$) and two remote devices ($N_r = 2$). The general architecture can be decomposed into two layers: 1) a *Transparency Layer* and 2) a *Passivity Layer*. In the transparency layer, local and remote side exchange position, velocity, and force information that are used for computing the desired inputs ($F_{l_1}^d$, $F_{l_2}^d$, $F_{r_1}^d$, $F_{r_2}^d$). These forces are sent to the passivity layer whose role is to passively implement them using the energy stored in the tanks. Local and remote energy tanks can exchange power for balancing the amount of energy stored at both local and remote sides.

It is worth noting that the $N_r - N_l$ autonomous arms are connected to the remote side tank to passively implement their control actions. Formally, the overall architecture with N_l^f admittance causality local devices, N_l^v impedance causality local devices, N_r^f admittance causality remote devices, and N_r^v impedance causality remote devices, and one tank per side can be modeled as (47), shown at the bottom of the next page, where $P_l^{\text{in}}, P_r^{\text{in}} \geq 0$ and $P_l^{\text{out}}, P_r^{\text{out}} \geq 0$ are incoming and outgoing power flows that the tanks can exchange with each other through the communication channel.

The interconnection between the two sides of the teleoperation system can be represented by

$$\begin{cases} P_r^{\text{in}}(t) &= P_l^{\text{out}}(t - \delta) \\ P_l^{\text{in}}(t) &= P_r^{\text{out}}(t - \delta) \end{cases} \tag{48}$$

where δ is the communication delay. For ease of notation, we consider that the communication delay is constant over time and the same in both directions. All the results can be extended to the time-varying case exploiting the strategy illustrated in [28].

The policy used to define P_l^{out} and P_r^{out} in (47) is

$$\begin{cases} P_l^{\text{out}}(t) &= (1-\sigma_l)\Big(\Big(\dot{x}_l^f\Big)^T D_l^f \dot{x}_l^f - x_{t_l}\Big(\omega_l^f\Big)^T \dot{x}_l^f + \\ &\quad -x_{t_l}\big(\omega_l^v\big)^T F_l^v\Big) + E_r^{\text{req}}(t-\delta)\beta_l \bar{P} \\ P_r^{\text{out}}(t) &= (1-\sigma_r)\Big(\Big(\dot{x}_r^f\Big)^T D_r^f \dot{x}_r^f - x_{t_r}\Big(\omega_r^f\Big)^T \dot{x}_r^f + \\ &\quad -x_{t_r}\big(\omega_r^v\big)^T F_r^v\Big) + E_r^{\text{req}}(t-\delta)\beta_r \bar{P} \end{cases} \tag{49}$$

where $\bar{P} \in \mathbb{R}_0^+$ is a design parameter which represents a rate of energy flowing from one tank to the other, and the flags E_l^{req}, E_r^{req} are used to implement an energy request process and are defined as

$$E_s^{\text{req}} = \begin{cases} 1, & \text{if } T_s\big(x_{t_s}\big) \le T_s^{\text{req}} \\ 0, & \text{otherwise.} \end{cases} \tag{50}$$

If the energy stored in the tank is under the user-defined threshold $T_s^{\text{req}} \in \mathbb{R}$ then the tank sends an energy request signal E_s^{req} to the other tank, which can provide energy to the other side under the following condition:

$$\beta_s = \begin{cases} 1, & \text{if } T_s\big(x_{t_s}\big) \ge T_s^{\text{ava}} \\ 0, & \text{otherwise} \end{cases} \tag{51}$$

namely, each tank can provide energy to the other side if the energy stored is over the user-defined threshold $T_s^{\text{ava}} \in \mathbb{R}$.

It is worth noting that the definition of the shared energy tank is slightly different with respect to the one in (23). This is because the introduction of the ports P_l^{in}, P_r^{in}, and P_l^{out}, P_r^{out} allow to share the power provided by the controller between the tanks, increasing the promptness of the overall system.

Through a revised use of these ports, compared to [4], the new formulation of the shared energy tank (6), and the new definition of σ_l and σ_r in (24) allow a more efficient use of energy within the entire teleoperation system. In fact, in case $\sigma_l = 0$, from (47) it results

$$\dot{x}_{t_l} = \frac{\Big(\dot{x}_l^f\Big)^T D_l^f \dot{x}_l^f}{x_{t_l}} - \Big(\omega_l^f\Big)^T \dot{x}_l^f - \big(\omega_l^v\big)^T F_l^v - \frac{P_l^{\text{out}}}{x_{t_l}}. \tag{52}$$

Substituting (49) in (52) it follows that:

$$\dot{x}_{t_l} = -\frac{E_r^{\text{req}}(t-\delta)\beta_l \bar{P}}{x_{t_l}} \tag{53}$$

which means that the energy in the tank can only decrease and the power dissipated by the damping and the one introduced by the operator action is transferred through P_l^{out} to the other side. Moreover, the input power is canceled out to avoid energy storage in the communication channel. Otherwise, if $\sigma_l = 1$, from (47) it results that

$$\dot{x}_{t_l} = \frac{\Big(\dot{x}_l^f\Big)^T D_l^f \dot{x}_l^f + P_l^{\text{in}}}{x_{t_l}} - \Big(\omega_l^f\Big)^T \dot{x}_l^f - \big(\omega_l^v\big)^T F_l^v + - \frac{E_r^{\text{req}}(t-\delta)\beta_l \bar{P}}{x_{t_l}} \tag{54}$$

which means that the tank doesn't need to be upper-bounded and all the power sources can interact with it. The same behavior holds for the remote side. This process did not occur in [4], as the terms σ_l and σ_r were used to redirect only the power due to damping. In such cases, when the energy stored in the tank needs to be upper-bounded, the power introduced by the operator is always wasted instead of being shared with the other side. This new mechanism of managing the power flowing to/from the tanks decreases the conservativeness of the overall teleoperation architecture.

A. Passivity of the Overall Architecture

The strategy illustrated so far guarantees the passivity of the teleoperation system as we will prove in this subsection. At first, we need to guarantee that the new definition of $P_s^{\text{out}}(t)$ still satisfies the condition described in [4], as the following lemma states.

Lemma 1: $P_s^{\text{out}}(t) \ge 0$ with $s \in \{l, r\}$.

Proof: Since $\sigma_s, E_s^{\text{req}}, \beta_s \in \{0, 1\}$ and $\bar{P} \ge 0$, we get

$$E_s^{\text{req}}(t-\delta)\beta_s \bar{P} \ge 0. \tag{55}$$

Thus, from (49) it follows that $P_s^{\text{out}}(t)$ is non-negative if and only if:

$$(1-\sigma_s)\Big(\Big(\dot{x}_s^f\Big)^T D_s^f \dot{x}_s^f - x_{t_s}\Big(\omega_s^f\Big)^T \dot{x}_s^f\Big) - x_{t_s}\big(\omega_s^v\big)^T F_s^v\Big) \ge -E_s^{\text{req}}(t-\delta)\beta_s \bar{P}. \tag{56}$$

If $\sigma_s = 1$, (56) becomes

$$-E_s^{\text{req}}(t-\delta)\beta_s \bar{P} \le 0 \tag{57}$$

that is always true thanks to (55). If $\sigma_s = 0$, from (24) we have

$$\Big(\Big(\dot{x}_s^f\Big)^T D_s^f \dot{x}_s^f - x_{t_s}\Big(\omega_s^f\Big)^T \dot{x}_s^f\Big) - x_{t_s}\big(\omega_s^v\big)^T F_s^v) \ge 0 \tag{58}$$

$$\begin{cases} \Lambda_l^f\ \ddot{x}_l^f + \mu_l^f\ \dot{x}_l^f + D_l^f\ \dot{x}_l^f = \omega_l^f\ x_{t_l} + E_l^f \\ \Lambda_l^v\ \ddot{x}_l^v + \mu_l^v\ \dot{x}_l^v = F_l^v\big(\omega_l^v\ x_{t_l}\big) + E_l^v \\ \dot{x}_{t_l} = \dfrac{\Big(\dot{x}_l^f\Big)^T\ D_l^f\ \dot{x}_l^f + \sigma_l P_l^{\text{in}}}{x_{t_l}} - \Big(\omega_l^f\Big)^T\ \dot{x}_l^f - \big(\omega_l^v\big)^T\ F_l^v - \dfrac{P_l^{\text{out}}}{x_{t_l}} \\ \Lambda_r^f\ \ddot{x}_r^f + \mu_r^f\ \dot{x}_r^f + D_r^f\ \dot{x}_r^f = \omega_r^f\ x_{t_r} + E_r^f \\ \Lambda_r^v\ \ddot{x}_r^v + \mu_r^v\ \dot{x}_r^v = F_r^v\big(\omega_r^v\ x_{t_r}\big) + E_r^v \\ \dot{x}_{t_r} = \dfrac{\Big(\dot{x}_r^f\Big)^T\ D_r^f\ \dot{x}_r^f \sigma_r P_r^{\text{in}}}{x_{t_r}} - \Big(\omega_r^f\Big)^T\ \dot{x}_r^f - \big(\omega_r^v\big)^T\ F_r^v - \dfrac{P_r^{\text{out}}}{x_{t_r}} \end{cases} \tag{47}$$

which satisfy (56). This is the only case where the input term contributes to $P_s^{\text{out}}(t)$. As a consequence, $P_s^{\text{out}} \geq 0$ and this proves the lemma. □

We are now ready to state the main result.

Proposition 2: The MLMR teleoperation system in (47) is passive with respect to the pair $((E_{l_1}^f, \ldots, E_{l_{N_l^f}}^f, E_{l_1}^v, \ldots, E_{l_{N_l^v}}^v, E_{r_1}^f, \ldots, E_{r_{N_r^f}}^f, E_{r_1}^v, \ldots, E_{l_{N_r^v}}^v), (\dot{x}_{l_1}^f, \ldots, \dot{x}_{l_{N_l^f}}^f, \dot{x}_{l_1}^v, \ldots, \dot{x}_{l_{N_l^v}}^v, \dot{x}_{r_1}^f, \ldots, \dot{x}_{r_{N_r^f}}^f, \dot{x}_{r_1}^v, \ldots, \dot{x}_{r_{N_r^v}}^v))$.

Proof: We consider as storage function the total energy of the teleoperation system

$$W(t) = V_l^f(t) + V_l^v(t) + V_r^f(t) + V_r^v(t) + T_l(t) + T_r(t) + H_{ch}(t) \tag{59}$$

where $H_{ch}(t)$ is the energy stored in the communication channel.

Using (47), we have that

$$\begin{aligned}\dot{W}(t) = {} & x_{t_l}\left(\omega_l^f\right)^T \dot{x}_l^f + \left(\dot{x}_l^f\right)^T E_l^f - \left(\dot{x}_l^f\right)^T D_l^f \dot{x}_l^f \\ & + x_{t_l}\left(\omega_l^v\right)^T F_l^v + \left(\dot{x}_l^v\right)^T E_l^v \\ & + x_{t_r}\left(\omega_r^f\right)^T \dot{x}_r^f + \left(\dot{x}_r^f\right)^T E_r^f - \left(\dot{x}_r^f\right)^T D_r^f \dot{x}_r^f \\ & + x_{t_r}\left(\omega_r^v\right)^T F_r^v + \left(\dot{x}_r^v\right)^T E_r^v \\ & + \left(\dot{x}_l^f\right)^T D_l^f \dot{x}_l^f - x_{t_l}\left(\omega_l^f\right)^T \dot{x}_l^f - x_{t_l}\left(\omega_l^v\right)^T F_l^v \\ & + \sigma_l P_l^{\text{in}}(t) - P_l^{\text{out}}(t) \\ & + \left(\dot{x}_r^f\right)^T D_r^f \dot{x}_r^f - x_{t_r}\left(\omega_r^f\right)^T \dot{x}_r^f - x_{t_r}\left(\omega_r^v\right)^T F_r^v \\ & + \sigma_r P_r^{\text{in}}(t) - P_r^{\text{out}}(t) + \dot{H}_{ch}(t).\end{aligned} \tag{60}$$

While the power is traveling from one side to the other, it is stored in the communication channel that becomes an energy-storing element in the teleoperation system. In particular, as shown in [29], we have that

$$H_{ch}(t) = \int_{t-\delta}^{t} \left(P_l^{\text{out}}(\tau) + P_r^{\text{out}}(\tau)\right) d\tau. \tag{61}$$

From (61) we get

$$\dot{H}_{ch}(t) = P_l^{\text{out}}(t) - P_l^{\text{out}}(t-\delta) + P_r^{\text{out}}(t) - P_r^{\text{out}}(t-\delta) \tag{62}$$

and considering (48) and replacing (62) in (60) we end up with

$$\begin{aligned}\dot{W}(t) = {} & \left(\dot{x}_l^f\right)^T E_l^f + \left(\dot{x}_l^v\right)^T E_l^v + \left(\dot{x}_r^f\right)^T E_r^f + \left(\dot{x}_r^v\right)^T E_r^v \\ & - (1-\sigma_l) P_l^{\text{in}}(t) - (1-\sigma_r) P_r^{\text{in}}(t).\end{aligned} \tag{63}$$

Since $\sigma_s \in \{0, 1\}$ and from Lemma 1, $P_s^{\text{in}} \geq 0$, it follows that:

$$\dot{W}(t) \leq \left(\dot{x}_l^f\right)^T E_l^f + \left(\dot{x}_l^v\right)^T E_l^v + \left(\dot{x}_r^f\right)^T E_r^f + \left(\dot{x}_r^v\right)^T E_r^v \tag{64}$$

hence

$$\begin{aligned}\dot{W}(t) \leq {} & \sum_{i=1}^{N_l^f} \left(\dot{x}_{l_i}^f\right)^T E_{l_i}^f + \sum_{j=1}^{N_l^v} \left(\dot{x}_{l_i}^v\right)^T E_{l_i}^v \\ & + \sum_{i=1}^{N_r^f} \left(\dot{x}_{r_i}^f\right)^T E_{r_i}^f + \sum_{j=1}^{N_l^v} \left(\dot{x}_{r_i}^v\right)^T E_{r_i}^v\end{aligned} \tag{65}$$

which implies the passivity condition

$$\begin{aligned}W(t) - W(0) \leq {} & \int_0^t \sum_{i=1}^{N_l^f} \left(\dot{x}_{l_i}^f(\tau)\right)^T E_{l_i}^f(\tau) \\ & + \sum_{j=1}^{N_l^v} \left(\dot{x}_{l_i}^v(\tau)\right)^T E_{l_i}^v(\tau) + \sum_{i=1}^{N_r^f} \left(\dot{x}_{r_i}^f(\tau)\right)^T E_{r_i}^f(\tau) \\ & + \sum_{j=1}^{N_l^v} \left(\dot{x}_{r_i}^v(\tau)\right)^T E_{r_i}^v(\tau) d\tau.\end{aligned} \tag{66}$$

□

Remark 1: The architecture has been proposed in a continuous time setting. To implement the architecture on a digital control system, discretization is needed. It is well known (see e.g., [28]) that a naive discretization of a passivity-based controller can lead to inaccuracies in the energy bookkeeping and even to a loss of passivity. Nevertheless, these effects can be made negligible using control frequencies much higher than the mechanical dynamics or using passive sampling as proposed in [28] and [30].

V. Preliminary Simulations

Due to the difficulty of evaluating the differences between the novel tank dynamics proposed in Section III and its classical definition [4], we perform the comparison in a simulated environment, and so, more easily controllable. We also decide to simplify the robot model and use two rotational 1-DOF robotic manipulators (modeled as second-order dynamic systems) since the behavior of the tank does not depend on the number of DOFs. The interaction torque provided by the operator is modeled as a position proportional derivative (PD) controller where the inputs are the reference signal and the delayed position and velocity of the robot at the remote side. This feedback loop models the classic video streaming used in a real teleoperation setup, where the operator uses the perceived remote side robot position to control its haptic device. The transparency layer is built with two position PD controllers, while the passivity layer implements a basic heuristic where the desired command is implemented if and only if the corresponding tank has enough energy. The simulation has been developed using *Simulink* on *MATLAB R2022a*.

The test is conducted with a constant delay of 150 ms between the operator and the environment side. The energy thresholds $T^{\max} = 1.5$, $T^{\text{ava}} = 0.6$, $T^{\text{req}} = 0.4$, $\epsilon = 0.001$, $\bar{P} = 0.01$ are set to such values to force the local and the remote side tanks toward the upper and the lower bounds, respectively. The tanks are initialized to $T^{\max}/2$ at the local side and ϵ at the remote side. The robot model parameters (i.e., inertia and friction) are set equal to $j = 0.0266$ kgm^2 and $b = 0.0218$ Ns.

A. Behavior Comparison

As shown in Fig. 3(a) and (b) the tanks at the remote side are almost empty. The behavior of the tanks between 0 sec to 5 sec are the same since the increase of the stored energy is only driven by the energy sent through $\bar{P}$ from the local to

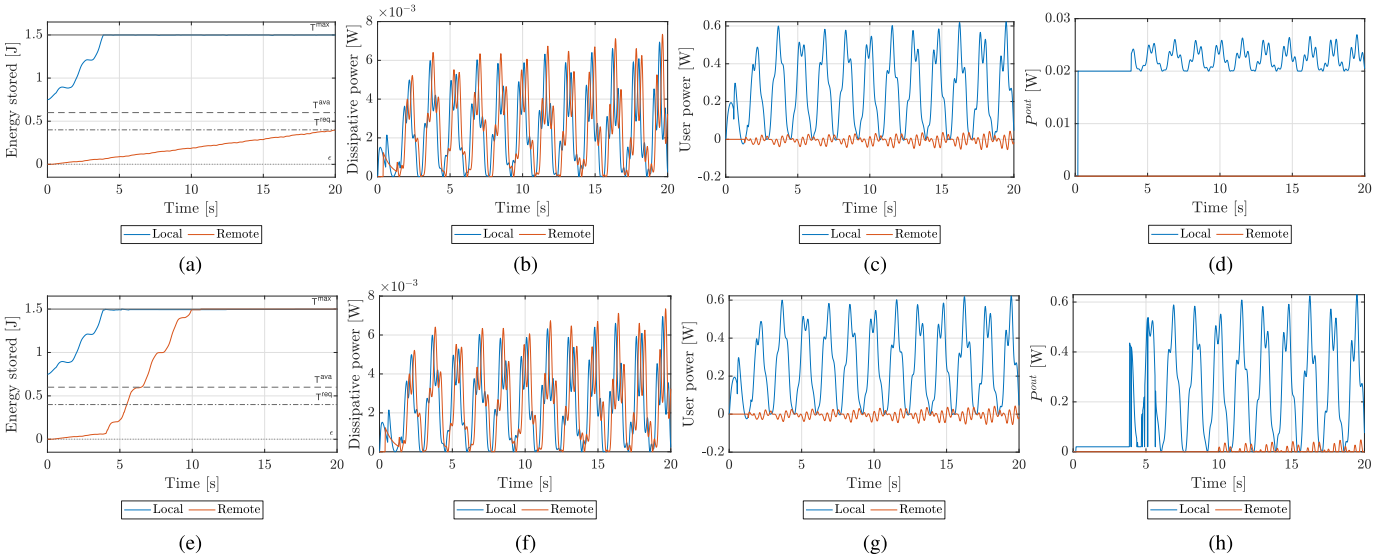

Fig. 3. Comparison of the classical and proposed tank dynamic's behavior. In red and blue are the local and remote side tanks respectively. (a) and (e) Evolution of the tanks. (b) and (c) Powers dissipated by the robots. (c) and (g) Powers generated by the control actions. (d) and (h) Output powers. (a)–(d) Results using the classical tank definition. (e)–(h) Results using the proposed tank definition.

the remote side. In both cases at 5 s, the teleoperated robots have enough energy to perform their control actions and start following the same trajectory. For this reason, as shown in Fig. 3(b), (c), (f), and (g), the dissipated powers and the powers provided by the controllers in the transparency layer are the same in both cases.

The effect of the proposed novel tank dynamics can be clearly seen by comparing Fig. 3(a) with Fig. 3(e). With the classical tank definition when the tank at the local side reaches its upper bound it starts to provide the dissipated power and $\bar{P}$ to the remote side tank. This results in a linear increase in the remote side tank until the E^{req} has been reached, around 20 s. On the other hand, our tank dynamics adds to the dissipated power and $\bar{P}$ also the power dissipated by the control action. In fact, as shown in Fig. 3(h), the power shared by the tank at the local side starting from 5 s includes the input power shown in Fig. 3(g). This additional power source, as shown in Fig. 3(e), increases the tank level at the remote side reaching the upper bound around 9 s.

The proposed solution can improve the promptness of the whole teleoperation system and guarantees a less conservative passivity margin.

VI. Experimental Evaluation

The proposed bilateral teleoperation architecture has been evaluated in a surgical scenario, performing the peg-and-ring [31] and the peg-in-hole [32] training tasks under a constant communication delay of 300 ms between the local and remote sides. As shown in Fig. 4, the experimental setup is composed of a Vinci[3] robot, controlled using the da Vinci research kit (dVRK), and a Franka Emika manipulator. The dVRK is the laboratory version of the Vinci[1] surgical robotic system [33]. The robot consists of two patient side manipulators (PSMs), each one equipped with 7-DOFs plus a gripper, two local tool manipulators (MTMs) and one endoscopic camera manipulator (ECM). For the aim of this article, we replaced

[3]Registered trademark.

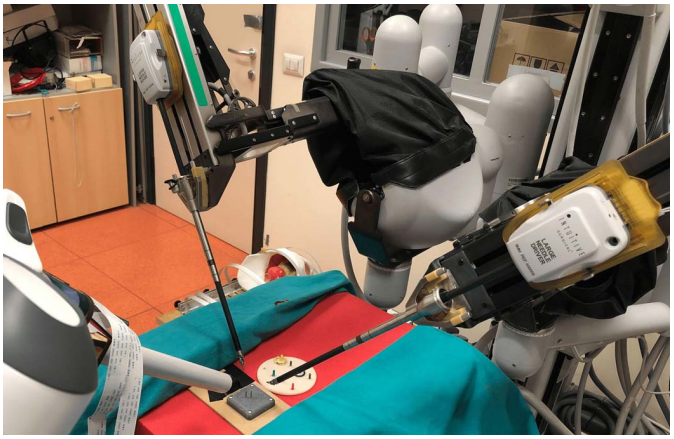

Fig. 4. Remote side of the experimental setup. The remote side of the teleoperation is composed of two PSMs together with the autonomous Franka Emika arm holding the stereo endoscope.

the standard endoscope with a custom-made stereo endoscope attached to a Franka Emika robot. In surgical applications like that the velocities are quite limited. This results in mechanical dynamics much slower than the control frequency, which in our case is of 1000 Hz.

The whole setup consists of a dual bilateral teleoperation (DMDS) system together with an autonomous camera controller in a shared-control fashion. At the local side, the two MTMs are connected to the same tank and they work with admittance causality. At the remote side, the two PSMs and the Franka Emika robot are still connected to the remote tank but with different causalities. In fact, the two PSMs are velocity-controlled and, therefore, present impedance causality, while the Franka Emika robot works with an admittance causality. This setup allows to harvest energy at the remote side without affecting the tracking performance of the PSMs. In fact, since they are velocity controlled, a variation of their desired velocities to produce artificial damping would affect the overall transparency. This can be avoided, at the remote

TABLE I
CONFIGURATION OF THE LOCAL SIDE AND REMOTE SIDE TANK USED FOR THE EXPERIMENTAL EVALUATION

Parameter	Local side tank (J)	Remote side tank (J)
T_s^{max}	5.0	5.0
T_s^{min}	0.01	0.01
$T_s^{b_{max}}$	3.5	2.0
$T_s^{b_{min}}$	0.1	0.1
T_s^R	1.5	1.5
T_s^{ava}	2.5	2.0
T_s^{req}	1.0	1.0
$\bar{P}$	0.05	0.05

side, by injecting artificial damping to only the Franka Emika arm. It is worth mentioning that the clutch system of the dVRK local console allows us to deal with the position drift introduced by the modulation (31) of the remote robots.

The tanks' parameters are reported in Table I. We chose to set the same energy upper-bound $T_s^{\max}$ since the energy consumption of all manipulators is similar. Regarding the artificial damping D_s^f, we set a higher threshold $T_s^{b_{\max}}$ at the local side since the manipulators are always in interaction with the user from whom we can harvest energy without degrading the tracking performance. For the same reason, we also set a higher value for T_s^{ava}. For both tanks, the modulation threshold T_s^R is set to be smaller than T_s^{ava} to not have a local performance degradation to satisfy the remote energy requests.

The peg-and-ring task consists of placing rings on the same-colored pegs, using the two PSMs. Even if peg-and-ring is not a proper surgical task, it is widely used as a training exercise for surgeons, since it presents many challenges in common with real surgery, like avoiding obstacles, grasping, and positioning small objects with precision and dexterity (like needle grasping in suturing) [31]. In the peg-in-hole task, the user must insert two small metal pegs into a set of holes having different tolerances with respect to the nominal peg's diameter. This would cause different values of force feedback during the peg insertion. Since the peg-and-ring requires almost no interaction with the environment we will assume a free-motion condition, while the peg-in-hole is used to evaluate the performance in contact condition.

The Franka Emika robot is controlled using a position PD controller with *variable stiffness*. The target position for the controller is the middle point between the two PSMs' end-effectors, while the orientation is computed such that the endoscope points always toward that point. The operator can regulate the target distance along the pointing direction during the experiment. In our application, the stiffness of the controller is inversely proportional to such distance. This choice is justified by the fact that for high distances a high tracking quality is not necessary as the field of view is wide. Conversely, for small distances, it is necessary to correctly track the target to keep the surgical instruments in sight. The variation of stiffness during the experiments is shown in Fig. 5. Since the variable stiffness controller is implemented within the transparency layer, the energy level at the remote side is monitored by the tank as in (9), and thus

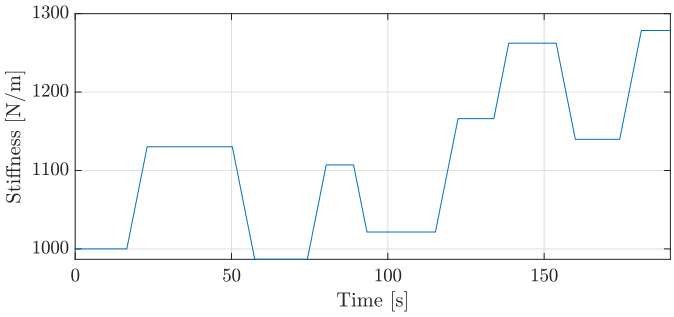

Fig. 5. Variation of the Franka Emika controller's parameters during the experimental evaluation.

the energy contribution introduced by the stiffness variation is intrinsically included in the energy balance by measuring ${}^{\tau}F_{r_1}^f$ and ${}^{\tau}\dot{x}_{r_1}^f$. This highlights the high level of flexibility of this approach: the user can freely choose the desired action and the system will take care of implementing it as faithfully as possible accordingly to passivity.

A. Transparency Layer

In the setup presented so far, at the local side we have $N_l^f = 2$ for the two MTMs, and $N_l^v = 0$, while at the remote side we have $N_r^f = 1$ for the Franka Emika robot holding the endoscope, and $N_r^v = 2$ for the PSMs. The transparency layer provides each side of the teleoperation system with the desired command. At the local side, we modeled the transparency layer as a virtual-damped spring linking the MTMs and the PSMs as

$$\begin{cases} {}^{\text{des}}F_{l_1}^f(t) &= K_{l_1}^p e_{l_1}(t) + K_{l_1}^d \dot{e}_{l_1}(t) \\ {}^{\text{des}}F_{l_2}^f(t) &= K_{l_2}^p e_{l_2}(t) + K_{l_2}^d \dot{e}_{l_2}(t) \end{cases} \tag{67}$$

where ${}^{\text{des}}F_{l_1}^f(t)$ is the MTM1 desired force and ${}^{\text{des}}F_{l_2}^f(t)$ is the MTM2 desired force. The transparency policy is modulated through the proportional semi-positive definite gain matrices $K_{l_1}^p$ and $K_{l_2}^p$ and by the derivative semi-positive definite gain matrices $K_{l_1}^d$ and $K_{l_2}^d$. The tracking errors are defined as

$$\begin{cases} e_{l_1}(t) &= x_{r_1}^v(t-\delta) - x_{l_1}^f(t) \\ e_{l_2}(t) &= x_{r_2}^v(t-\delta) - x_{l_2}^f(t). \end{cases} \tag{68}$$

Due to the delay introduced by the communication channel, the desired force for the local devices is necessarily computed using delayed information.

To guarantee a small tracking error at the remote side, we modeled the transparency layer as

$$\begin{cases} {}^{\text{des}}\dot{x}_{r_1}^v(t) &= \dot{x}_{l_1}^f(t-\delta) \\ {}^{\text{des}}\dot{x}_{r_2}^v(t) &= \dot{x}_{l_2}^f(t-\delta) \\ {}^{\text{des}}F_{r_1}^f(t) &= K_{r_1}^p(t) e_{r_1}(t) + K_{r_1}^d(t) \dot{e}_{r_1}(t) \end{cases} \tag{69}$$

where ${}^{\text{des}}\dot{x}_{r_1}^v(t)$ and ${}^{\text{des}}\dot{x}_{r_2}^v(t)$ represents the desired velocity for the PSM1 and the PSM2, respectively, and ${}^{\text{des}}F_{r_1}^f(t)$ is the

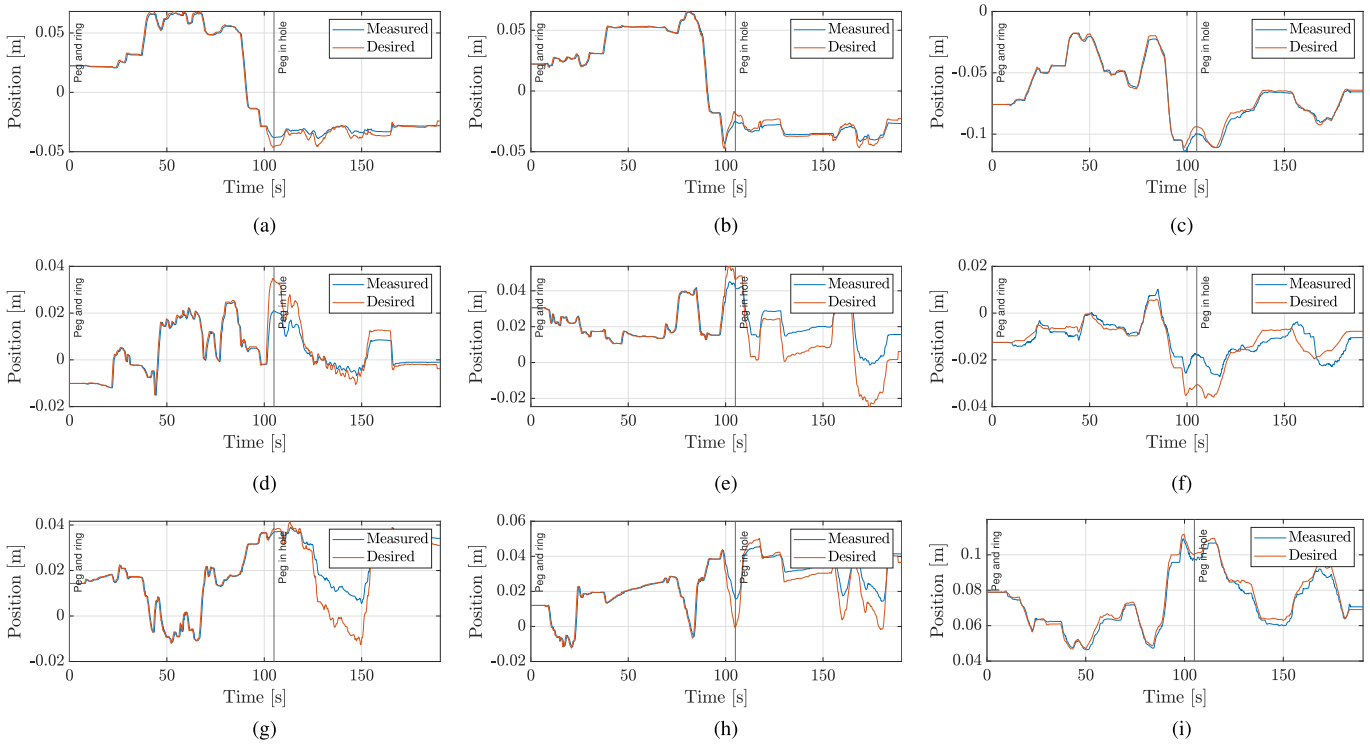

Fig. 6. Position tracking on x–z axes for the remote side manipulators. In blue and orange the measured and the desired position, respectively. The position tracking degrades during the peg-in-hole task due to the environment interaction and the effect of the tank modulation. (a) PSM1, (b) PSM2, and (c) Franka Emika x axis. (d) PSM1, (e) PSM2, and (f) Franka Emika y axis. (g) PSM1, (h) PSM2, and (i) Franka Emika z axis.

desired force for the Franka Emika robot with

$$e_{r_1}(t) = {}^{\text{des}}x^f_{r_1}(t) - x^f_{r_1}(t) \tag{70}$$

where ${}^{\text{des}}x^f_{r_1}$ is the desired position for the endoscope provided by the autonomous controller. The desired force for the Franka Emika robot ${}^{\text{des}}F^f_{r_1}$ depends also on the time-varying semi-definite proportional and derivative gain matrices $K^p_{r_1}(t)$ and $K^d_{r_1}(t)$ which are adjusted to control the endoscope accuracy with respect to the viewing distance.

B. Results

The tracking performance of the remote devices is shown in Fig. 6. The tracking error of the PSMs is always within few millimeters for almost all the peg-and-ring experiment, $t >$ 105 s, while it increases significantly during the peg-in-hole experiment, $t >$ 105 s. This is due to two reasons: 1) during the second part of the experiment the manipulators are often in contact with the environment and 2) the tank's energy value is always below the modulation threshold T^R_r. Anyhow, the proposed teleoperation system allows us to always carry out the two training tasks, as shown in the accompanying video. The evolution of the two tanks is shown in Fig. 7: the energy stored in the remote tank is constantly larger than the threshold T^R_s up to $t = 97.5$ s. After that, the tank starts to modulate the desired input (i.e., the desired velocities for the PSM1 and PSM2 and the desired forces for the Franka Emika robot) to prevent emptying the tank and guarantee the passivity of the system. This causes a higher tracking error during the final part of the peg-and-ring task, as shown in Table II, and for the whole duration of the peg-in-hole experiment, as shown in Fig. 6.

TABLE II

MODULATION EFFECT ON THE RMSE OF THE TRACKING ERROR DURING THE PEG-AND-RING FOR THE PSM1, PSM2, AND THE FRANKA EMIKA ARMS (x–z AXES)

Arm	Nominal (mm)	Modulated (mm)
PSM1	(2.1,1.8,1.5)	(5.2,9.6,0.95)
PSM2	(2.0,1.3,1.8)	(5.8,7.3,10.2)
Franka Emika	(1.4,2.2,2.2)	(5.5,11.3,3.2)

This is also confirmed by the behavior of the desired velocity, the modulated velocity, and the real velocity shown in Fig. 8. In fact, the modulated and the desired velocities coincide as long as the energy in the remote tank remains above the threshold T^R_r. For the Franka Emika robot, as shown in Fig. 6, such tracking degradation effects are visible only during the dynamic phases because the manipulator has an admittance causality. This means that the robot is controlled by providing desired forces and the modulation acts directly on them. Furthermore, the quality of the tracking, in this case, depends also on the implemented control law, i.e., PD with variable coefficients and with not a particularly high stiffness to ensure smooth transients of the image. Fig. 9 shows the effects of the forces modulation.

Similar considerations apply to the MTMs, whose desired and modulated forces are shown in Fig. 10. In this case, the energy stored in the local tank never goes below the threshold T^R_m and so the modulation is never applied for the whole experiment's duration. The root-mean-square error (RMSE) of the force tracking error is 0.07 and 0.09 N for the MTM1 and the MTM2, respectively.

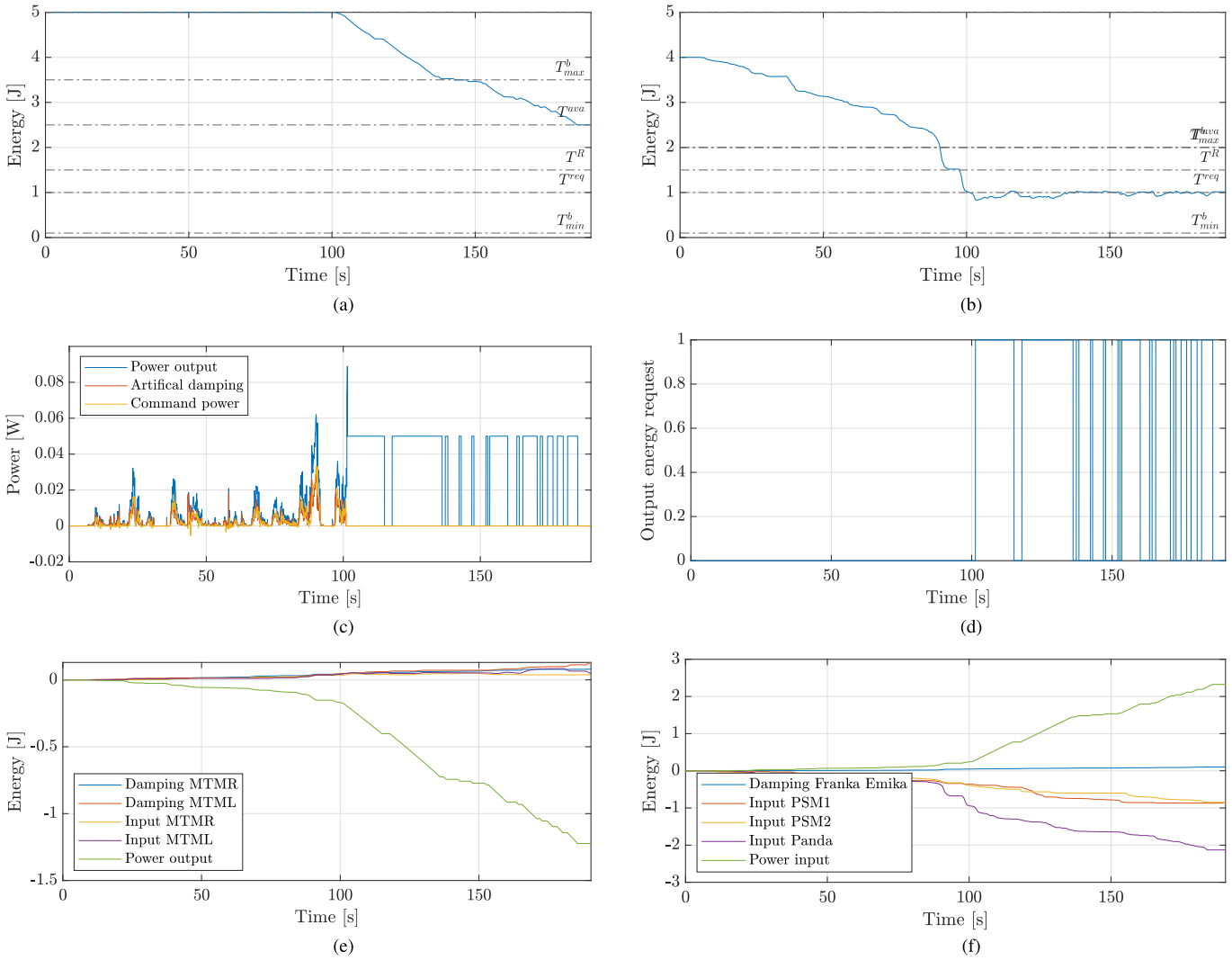

Fig. 7. Tank dynamics of both sides of the teleoperation. The local tank input power and energy requests together with the remote tank output power and input energy requests are not reported since they are always zero. (a) Local and (b) remote tank dynamics. (c) Local tank output powers. (d) Remote tank energy requests. (e) Local and (f) remote tank contributions.

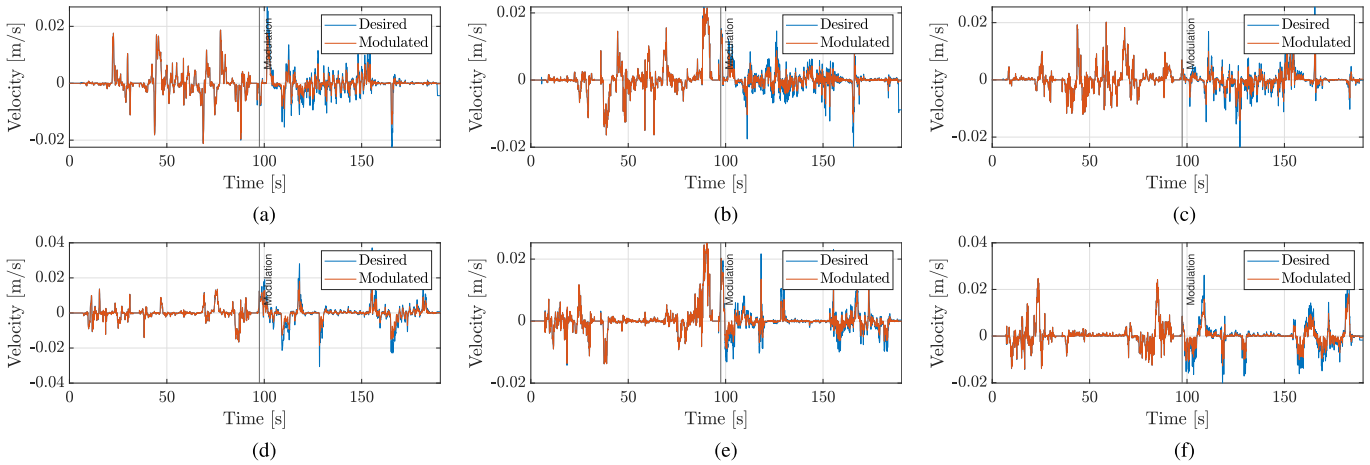

Fig. 8. Velocity modulation on x–z axes for the PSMs. In blue and orange the desired and the modulated position, respectively. The modulation of the desired velocities is due only to the action of the passivity layer since the two manipulators are in an admittance causality. PSM1 (a) x axis, (b) y axis, and (c) z axis. PSM2 (d) x axis, (e) y axis, and (f) PSM2 z axis.

The effect of the novel tank dynamic, applied to the energy transfer protocol, can be seen in Fig. 7(c). In fact, as opposed to [4], until the local tank stays at its upper-bound (for $t >$ 100 s) the transferred output power is the power of the artificial

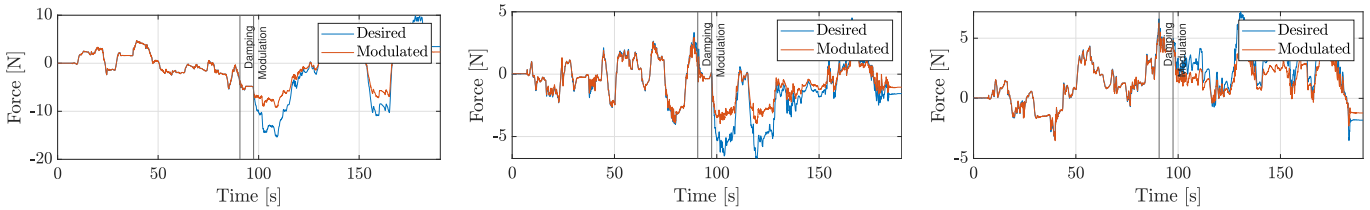

Fig. 9. Force modulation on x–z axes for the endoscope arm. In blue and orange the desired and the modulated force, respectively. The modulation of the desired control forces is both due to the artificial damping and the action of the passivity layer. Franka Emika (a) x axis, (b) y axis, and (c) z axis.

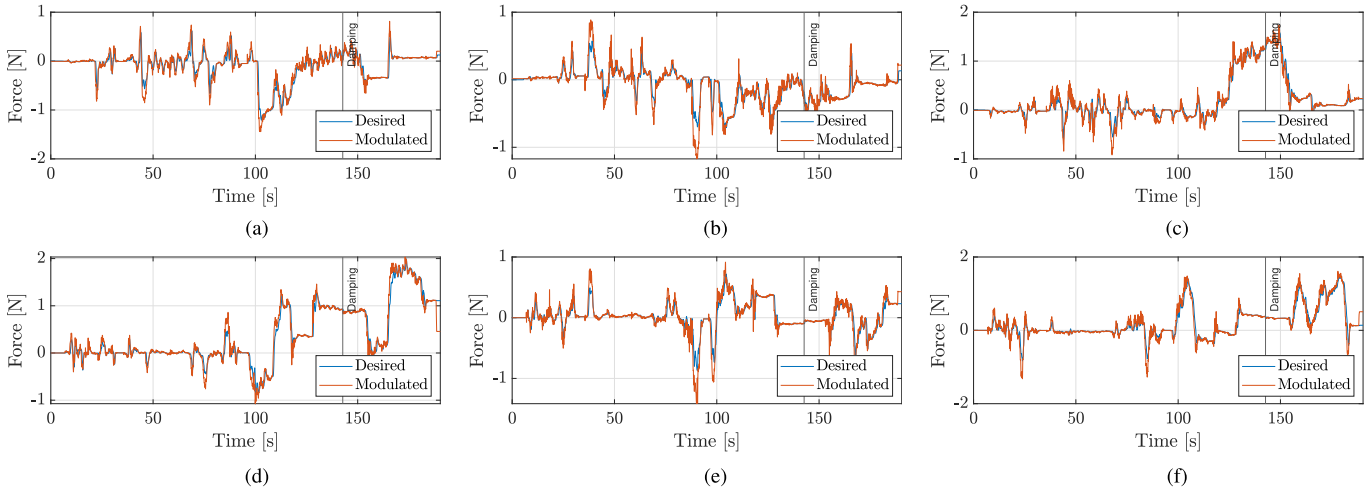

Fig. 10. Force modulation on x–z axes for the MTMs. In blue and orange the desired and the modulated position, respectively. The modulation of the desired control forces is due only to the artificial damping since the tank at the operator side never reaches the modulation threshold. MTM1 (a) x axis, (b) y axis, and (c) z axis. MTM2 (d) x axis, (e) y axis, and (f) z axis.

damping together with the novel addition of the input power. This leads to, as shown in Fig. 3, higher energy recycling while guaranteeing the proper tank bound. Once the local tank goes below $T_l^{\max}$ (for $t > 100$ s), the energy transferred to the remote tank is due to the energy request mechanism only, i.e., when the energy request E_r^{req} is sent by the remote tank to the local tank. Since the local tank has more energy than the T_l^{ava} threshold, it provides such energy through the power port P_l^{out} by means of the energy packets $\bar{P}$. Finally, Fig. 7(e) and (f) show the energy contributions of each manipulator in the dynamics of the tank. The contribution of the damping at the local side increases the energy stored in the tank to guarantee the correct functioning of the system. Moreover, it provides a sufficient overall energy level within the teleoperation system and at the same time, it is not intrusive for the operator, who does not see the desired force feedback much altered. The major contribution of energy in the system is the one introduced by the power exchange between the two sides of the teleoperation architecture. Sharing the energy between the two sides of the teleoperation architecture allows the overall system to reduce the whole conservativeness and avoid situations where one of the sides can be stuck without energy.

VII. Conclusion

In this article, we improved the shared energy tank by designing an upper-bounding system based on the exchange of energy between the two sides of the teleoperation system. This reduces conservativeness and improves transparency while guaranteeing passivity. The new architecture has been validated with a surgical robot on training tasks. Moreover, the teleoperation system has been augmented at the remote side with an autonomous robot. The arm holds the endoscope and always keeps the scene within the camera viewport. This underlines the flexibility of the architecture to handle both autonomous and teleoperated arms, with both admittance and impedance causality, within the same tank.

References

[1] J. Scholtz, M. Theofanos, and B. Antonishek, "Development of a test bed for evaluating human–robot performance for explosive ordnance disposal robots," in *Proc. 1st ACM SIGCHI/SIGART Conf. Hum.-Robot Interact. (HRI)*, 2006, pp. 10–17.

[2] B. T. Bethea et al., "Application of haptic feedback to robotic surgery," *J. Laparoendoscopic Adv. Surgical Techn.*, vol. 14, no. 3, pp. 191–195, Jan. 2004.

[3] D. A. Lawrence, "Stability and transparency in bilateral teleoperation," *IEEE Trans. Robot. Autom.*, vol. 9, no. 5, pp. 624–637, Oct. 1993.

[4] M. Minelli, F. Ferraguti, N. Piccinelli, R. Muradore, and C. Secchi, "An energy-shared two-layer approach for multi-master-multi-slave bilateral teleoperation systems," in *Proc. Int. Conf. Robot. Autom. (ICRA)*, May 2019, pp. 423–429.

[5] G. Niemeyer, C. Preusche, S. Stramigioli, and D. Lee, "Telerobotics," in *Springer Handbook of Robotics*, B. Siciliano and O. Khatib, Eds. Berlin, Germany: Springer, 2016, ch. 42.

[6] G. Niemeyer and J. J. E. Slotine, "Telemanipulation with time delays," *Int. J. Robot. Res.*, vol. 23, no. 9, pp. 873–890, 2004.

[7] P. Huang, P. Dai, Z. Lu, and Z. Liu, "Asymmetric wave variable compensation method in dual-master-dual-slave multilateral teleoperation system," *Mechatronics*, vol. 49, pp. 1–10, Feb. 2018.

[8] L.-Y. Hu, X. P. Liu, and G.-P. Liu, "The wave-variable teleoperator with improved trajectory tracking," in *Proc. IEEE ICCA*, Jun. 2010, pp. 322–327.

[9] S. Munir and W. J. Book, "Internet-based teleoperation using wave variables with prediction," *IEEE/ASME Trans. Mechatronics*, vol. 7, no. 2, pp. 124–133, Jun. 2002.
[10] B. Hannaford and J.-H. Ryu, "Time-domain passivity control of haptic interfaces," *IEEE Trans. Robot. Autom.*, vol. 18, no. 1, pp. 1–10, Feb. 2002.
[11] J.-H. Ryu, D.-S. Kwon, and B. Hannaford, "Stable teleoperation with time-domain passivity control," *IEEE Trans. Robot. Autom.*, vol. 20, no. 2, pp. 365–373, Apr. 2004.
[12] Y. Ye, Y.-J. Pan, and Y. Gupta, "A power based time domain passivity control for haptic interfaces," in *Proc. 48th IEEE Conf. Decis. Control (CDC) Held Jointly 28th Chin. Control Conf.*, Dec. 2009, pp. 7521–7526.
[13] Z. Chen, Y. J. Pan, J. Gu, and S. Forbrigger, "A novel multilateral teleoperation scheme with power-based time-domain passivity control," *Trans. Inst. Meas. Control*, vol. 40, no. 11, p. 3252–3262, 2018.
[14] O. J. Smith, "Closed control of loop with dead time," *Chem. Eng. Prog.*, vol. 53, no. 5, pp. 217–219, 1957.
[15] J.-Q. Huang and F. L. Lewis, "Neural-network predictive control for nonlinear dynamic systems with time-delay," *IEEE Trans. Neural Netw.*, vol. 14, no. 2, pp. 377–389, Feb. 2003.
[16] J.-J. E. Slotine and W. Li, "On the adaptive control of robot manipulators," *Int. J. Robot. Res.*, vol. 6, no. 3, pp. 49–59, 1987.
[17] K. B. Fite, M. Goldfarb, and A. Rubio, "Transparent telemanipulation in the presence of time delay," in *Proc. IEEE/ASME Int. Conf. Adv. Intell. Mechatronics (AIM)*, Jul. 2003, pp. 254–259.
[18] A. C. Smith and K. Van Hashtrudi-Zaad, "Neural network-based teleoperation using Smith predictors," in *Proc. IEEE Int. Conf. Mechatronics Autom.*, vol. 3, Jul. 2005, pp. 1654–1659.
[19] Z. Li, Y. Xia, D. Wang, D.-H. Zhai, C.-Y. Su, and X. Zhao, "Neural network-based control of networked trilateral teleoperation with geometrically unknown constraints," *IEEE Trans. Cybern.*, vol. 46, no. 5, pp. 1051–1064, May 2016.
[20] Y. Ji, D. Liu, and Y. Guo, "Adaptive neural network based position tracking control for dual-master/single-slave teleoperation system under communication constant time delays," *ISA Trans.*, vol. 93, pp. 80–92, Oct. 2019.
[21] A. M. Okamura, "Methods for haptic feedback in teleoperated robot-assisted surgery," *Ind. Robot, Int. J.*, vol. 31, no. 6, pp. 499–508, Dec. 2004.
[22] D. Prattichizzo, C. Pacchierotti, and G. Rosati, "Cutaneous force feedback as a sensory subtraction technique in haptics," *IEEE Trans. Haptics*, vol. 5, no. 4, pp. 289–300, Apr. 2012.
[23] M. Franken, S. Stramigioli, S. Misra, C. Secchi, and A. Macchelli, "Bilateral telemanipulation with time delays: A two-layer approach combining passivity and transparency," *IEEE Trans. Robot.*, vol. 27, no. 4, pp. 741–756, Aug. 2011.
[24] F. Ferraguti et al., "An energy tank-based interactive control architecture for autonomous and teleoperated robotic surgery," *IEEE Trans. Robot.*, vol. 31, no. 5, pp. 1073–1088, Oct. 2015.
[25] C. Secchi, A. Franchi, H. H. Bulthoff, and P. R. Giordano, "Bilateral teleoperation of a group of UAVs with communication delays and switching topology," in *Proc. IEEE Int. Conf. Robot. Autom.*, May 2012, pp. 4307–4314.
[26] V. Duindam and S. Stramigioli, "Port-based asymptotic curve tracking for mechanical systems," *Eur. J. Control*, vol. 10, no. 5, pp. 411–420, 2004.
[27] D. Lee and K. Huang, "Passive-set-position-modulation framework for interactive robotic systems," *IEEE Trans. Robot.*, vol. 26, no. 2, pp. 354–369, Apr. 2010.
[28] S. Stramigioli, C. Secchi, A. J. V. D. Schaft, and C. Fantuzzi, "Sampled data systems passivity and discrete port-Hamiltonian systems," *IEEE Trans. Robot.*, vol. 21, no. 4, pp. 574–587, Aug. 2005.
[29] F. Ferraguti, C. Secchi, and C. Fantuzzi, "A tank-based approach to impedance control with variable stiffness," in *Proc. IEEE Int. Conf. Robot. Autom.*, May 2013, pp. 4948–4953.
[30] M. De Stefano, R. Balachandran, and C. Secchi, "A passivity-based approach for simulating satellite dynamics with robots: Discrete-time integration and time-delay compensation," *IEEE Trans. Robot.*, vol. 36, no. 1, pp. 189–203, Feb. 2020.
[31] M. Ginesi, D. Meli, A. Roberti, N. Sansonetto, and P. Fiorini, "Autonomous task planning and situation awareness in robotic surgery," in *Proc. IEEE/RSJ Int. Conf. Intell. Robots Syst. (IROS)*, Oct. 2020, pp. 3144–3150.
[32] B. Hannaford, L. Wood, D. A. McAffee, and H. Zak, "Performance evaluation of a six-axis generalized force-reflecting teleoperator," *IEEE Trans. Syst., Man, Cybern.*, vol. 21, no. 3, pp. 620–633, May/Jun. 1991.
[33] P. Kazanzides, Z. Chen, A. Deguet, G. S. Fischer, R. H. Taylor, and S. P. DiMaio, "An open-source research kit for the da Vinci surgical system," in *Proc. IEEE Intl. Conf. Robot. Auto. (ICRA)*, Hong Kong, May 2014, pp. 6434–6439.

Open Access funding provided by 'Università degli Studi di Modena e Reggio Emilia' within the CRUI CARE Agreement